
# Caractérisation expérimentale des spectres de pression pariétale pour des couches limites turbulentes avec gradient de pression

E. Salze, C. Bailly, O. Marsden, E. Jondeau et D. Juvé
Ecole Centrale de Lyon, Centre Acoustique - bât. KCA, 36 avenue Guy de Collongue, 69134 Ecully Cedex, France
edouard.salze@ec-lyon.fr

Wall-pressure fluctuations beneath a turbulent boundary layer are investigated experimentally. Interest is focused on the spectral properties of wavevector-frequency spectra. The incompressible part of these spectra is well documented in the literature for zero pressure gradient flows. Few data is available for the case of turbulent boundary layers submitted to favorable or adverse pressure gradients. Direct measurements of both contributions to the wall-pressure spectra (wall-bounded turbulence and acoustic) have been demonstrated possible in a previous study [1], in the case of a zero-pressure-gradient turbulent boundary layer developing in a wind tunnel with rigid walls. For the present study, a new experimental facility including absorbing walls is used. A new antenna has been designed to measure wavevector-frequency spectra $\Phi(k_x,k_y,\omega)$. Preliminary results obtained with different values of the pressure gradient $\beta$ are briefly presented. A more detailed study is available [22].

# 1 Introduction

Wall pressure fluctuations induced by a turbulent boundary layer are investigated in this study, by directly measuring wall pressure wavevector-frequency spectra beneath a turbulent boundary layer in the presence of a pressure gradient. Motivation is the investigation of noise generated by the turbulent boundary layer [12, 9] as well as the prediction of interior noise, for aeronautical [23, 11] and more recently for automotive applications [14, 2]. Many experimental results have been reported over the past fifty years [13, 3], but mainly for the incompressible part of spectra and for zero-pressure-gradient turbulent boundary layers. Only a partial view is currently offered regarding pressure gradient effects [20, 4, 19]. The extraction of the acoustic part is also quite tricky, regardless of the means of the study, by numerical simulation [9] or by experiments [7, 1, 8].

In Arguillat *et al.* [1], a rotating microphone array has been used to estimate both the aerodynamic and the acoustic part of the wall pressure wavevector-frequency spectrum through an original post-processing. The results reported for a turbulent boundary layer at a Reynolds number $\mathrm{Re}_{\delta_2} = u_\tau \delta_2/\nu = 1716$ and at a moderate velocity $U_\infty = 44$ m.s$^{-1}$ have demonstrated the feasibility of this approach, where $u\tau$ is the friction velocity, $\delta_2$ the momentum thickness and $\nu$ the kinetic viscosity of the fluid. It has also been noticed that some improvements could be carried out in the future, regarding the test channel as well as the antenna.

A new channel has been designed for flow-acoustic measurements in the present work, which allows turbulent boundary layers in the presence of a pressure gradient to be considered. The flow can be varied from 25 to 100 m.s$^{-1}$, but only measurements at 50 m.s$^{-1}$ are reported in this communication. The microphone array is mounted on a rigid flat plate, but the roof of the test section channel can be inclined. A new disk antenna has been designed to extract wall pressure wavevector-frequency spectra. The paper is organized as follows. The experimental setup is described in section 2, an overview of data processing is given in section 3. Preliminary results are reported and briefly discussed in section 4. Concluding remarks are finally drawn in section 5.

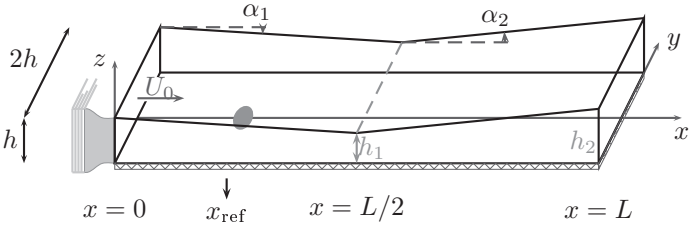


FIGURE 1 – Sketch of the test channel and notations. The height of the initial section is $h = 250$ mm, the length of the whole channel is $L = 16h$ and the location of the disk antenna is $x_{\mathrm{ref}} = 750$ mm. It should be noted that $U_0$ is the velocity at the channel inlet, an that $U_\infty$ is the local free stream velocity of the boundary layer at $x_{\mathrm{ref}}$.

# 2 Experimental setup

## 2.1 Wind tunnel

The experiments were conducted in the main subsonic wind tunnel of the Centre Acoustique at Ecole Centrale de Lyon in France [18, 1]. The flow is generated by a 350 kW Neu centrifugal blower delivering a nominal mass flow rate of 15 kg.s$^{-1}$, and the fan is powered by an electronically controlled Tridge-Electric LAK 4280A motor. Air passes through a settling chamber including a honeycomb and several wire meshes designed to reduce free stream turbulence. Acoustic treatment on the wind tunnel walls and baffled silencers allows to reduce the noise level and to prevent contamination of acoustic measurements performed in the anechoic chamber. This results in an air flow at ambient temperature with a low background noise and low residual turbulence intensity, less than 1%.

A sketch of the channel is shown in Figure 1. As mentioned in introduction, the two parts of the roof can be sloped to control the mean pressure gradient inside the channel. Three configurations have been retained in the present study, corresponding to a turbulent boundary layer submitted to a zero-pressure-gradient (ZPG), a favorable or negative pressure gradient (FPG) and an adverse or positive pressure gradient (APG). The geometrical parameters are provided in Table 1. The side walls of the second part of the channel have been acoustically treated using a wire mesh and a porous liner, in order to reduce noise generated by the jet at the channel outlet.

| Case | $\alpha_1$ | $\alpha_2$ | $h_1$ (cm) | $h_2$ (cm) | $U_0\|_{\max}$ |
|---|---|---|---|---|---|
| ZPG | 0.3° | 3.9° | 26.5 | 40 | 100 m.s$^{-1}$ |
| FPG | −3.5° | 1.5° | 12.75 | 18 | 50 m.s$^{-1}$ |
| APG | 4° | 4° | 39 | 51 | 100 m.s$^{-1}$ |

TABLEAU 1 – Parameters of the three configurations considered in this study, refer to Fig. 1 for the notations.

## 2.2 Wall-pressure instrumentation

The principle of a linear array placed on a rotating disk has been retained for this study, see Arguillat *et al.* [1], but the size of the disk has been slightly increased to obtain a better resolution of the low frequency components. Each remote probe is made of a 1/4 inch Brüel & Kjær type 4957 microphone, whose frequency cutoff is of about 15 kHz. The microphones are placed on the edge of steel tubes of variable diameter. The diameter of the last steel tubes, fit flush onto the surface of the rotating disk, has been set to 0.5 mm in order to reduce the spatial filtering. 2 m long rear tubes made of vinyl are used to dissipate pressure fluctuations and therefore avoid acoustical reflections. This mounting also reduces the spacing between two neighbour probes. The linear antenna consists of 63 identical remote microphone probes, in order to reach a spacing of 1 mm near the antenna center.

These probes are non-uniformly distributed along the disk diameter to optimize the antenna response. As an illustration of improvements of the new disk antenna, the antenna response is compared to the analytical solution for a pressure field composed of the sum of a diffuse spherical sound field [16], and of a Corcos model [5, 6] for the wall-bounded turbulence. The pressure cross-spectral density is given by the sum of these two contributions, respectively

$$\begin{aligned} R(\boldsymbol{r},\omega) &= R_a(\boldsymbol{r},\omega) + R_c(\boldsymbol{r},\omega) \\ &= S(\omega)\frac{\sin(k_0 r)}{k_0 r} \\ &\quad + A(\omega) e^{-(k_c/\alpha)|r_x|} e^{-(k_c/\beta)|r_y|} e^{ik_c r_x} \end{aligned}$$

where classical values have been chosen for the two constants, namely $\alpha = 8$, and $\beta = 1$. The numerical test is performed using a free stream velocity $U_\infty = 50$ m.s$^{-1}$ for the boundary layer, an arbitrary frequency $f = 2000$ Hz, a convective wavenumber $k_c = 2\pi f/U_c$ with $U_c \simeq 0.7U_\infty$, an acoustic wave number $k_0 = \omega/c_0$, $c_0$ being the sound celerity, and relative amplitudes $S = 1$ and $A = 10^{-3}$. The analytical wavenumber-frequency spectrum is respectively given by

$$\Phi_a(\boldsymbol{k},\omega) = \begin{cases} \dfrac{S(\omega)}{2\pi k_0^2} \dfrac{1}{\sqrt{1-(k/k_0)^2}} & \text{if } k < k_0 \\ 0 & \text{if } k > k_0 \end{cases} \quad (1)$$

and

$$\Phi_c(\boldsymbol{k},\omega) = \frac{A(\omega)}{\pi^2} \frac{\alpha k_c}{k_c^2 + \alpha^2(k_x - k_c)^2} \frac{\beta k_c}{k_c^2 + \beta^2 k_y^2} \quad (2)$$

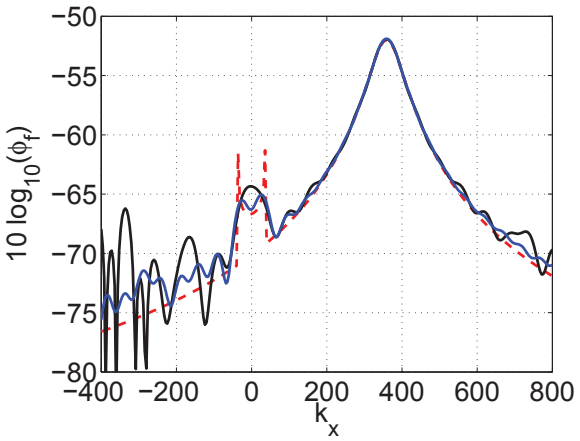


FIGURE 2 – Wavenumber spectrum, comparison between : ---- the analytical expression $\Phi_a(\boldsymbol{k},\omega) + \Phi_c(\boldsymbol{k},\omega)$ given by expressions (1) - (2), and —— the response given by the integration of expression (1) over the disk antenna used in Arguillat *et al.* [1] and —— for the microphone array used in this study.

In Figure 2, this analytical solution $\Phi_a(\boldsymbol{k},\omega) + \Phi_c(\boldsymbol{k},\omega)$ is compared to the response (1) provided by the antenna used in a previous study [1], and by the new antenna considered in the present work. A better resolution is obtained around the acoustic ridge. The spatial filtering [5, 15] induced by probes is negligible in this case, since $T_0(k_c d_p/2) \simeq 0.998$ where $T_0(\eta) = 2J_1(\eta)/\eta$ is the transfer function of the hole.

High-frequency measurement of frequency spectra is achieved by using a so-called *pinhole microphone*. The pinhole microphone is made of a 1/8 inch Brüel & Kjær type 4138 microphone, whose frequency cutoff is of about 140 kHz. The sensing area of the microphone has been reduced to 0.4 mm by fitting it with a pinhole mask, made of a perforated cap. The frequency cutoff of such a mounting is fixed by the frequency cutoff of the cavity inside the cap, which can be estimated as $f_0 = 1/2\pi\sqrt{3\pi d^2 c_0^2/16 L_H V_H}$, where $c_0$ is the speed of sound, $V_H$ is the volume of the pinhole cap, $d$ is the diameter of the hole, and $L_H$ is the length of the neck. With $c_0 = 340$ m/s, $V_H = 4$ mm$^3$, $d = 0.4$ mm and $L_H = 0.2$ mm, the resonance frequency is $f_0 = 23$ kHz.

The complex frequency responses H($\omega$) of the 63 remote probes are obtained in the range 10 Hz - 15 kHz using a loudspeaker mounted into a calibration tube. A flush-mounted 1/8 inch Brüel & Kjær type 4138 microphone is used as a reference microphone. The transfer function (in mV/Pa) of the first probe of the antenna is plotted in Fig. 3, where the different curves have been obtained at different times (approximately 10 days between each curve). A difference of about 5% is found, so the calibration process is not altered in time.

In order to calibrate the pinhole microphone in a high-frequency domain (15 kHz - 50 kHz), a second calibration method has been applied on the basis of previous studies [21, 17]. An electrical spark source is used to generate short duration and high pressure shock waves. The transfer function of the pinhole microphone

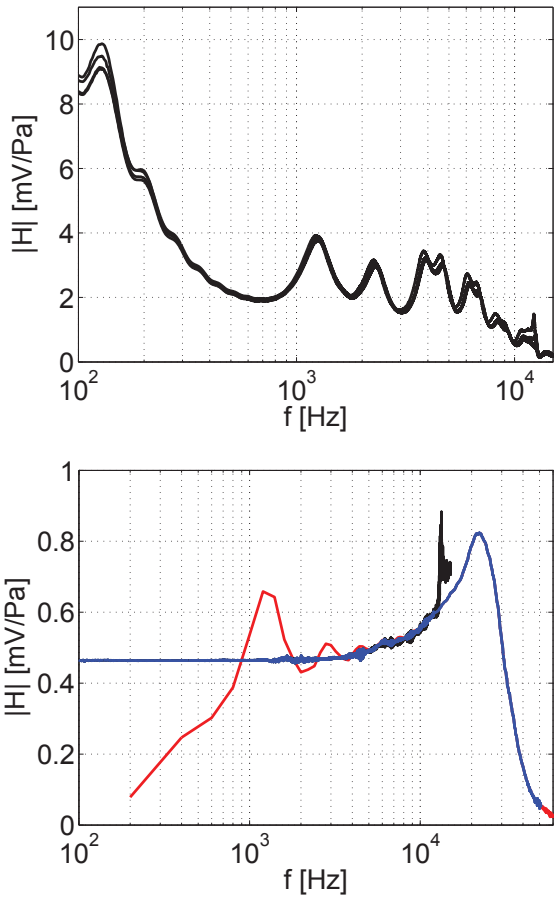


FIGURE 3 – Transfer function of the wall-pressure sensors. Above : transfer function of the first remote probe of the disk antenna, measured at different days. Below : transfer function of the pinhole microphone, —— obtained with a white noise source in the range 10 Hz - 12 kHz, —— obtained with the spark source in the range 3 kHz - 50 kHz, —— final transfer function built to cover the whole frequency domain.

is obtained in comparison to a reference flush-mounted 1/8 inch Brüel & Kjær type 4138 microphone with a higher frequency cutoff. The final frequency response of the pinhole microphone is obtained by combining the low-frequency response obtained using the loudspeaker, and the high-frequency response obtained using the spark source, as shown by the blue curve displayed in Fig. 3.

## 2.3 Flow characterization

The mean static pressure $P_e$ has been measured using a Validyne dp15 transducer, and the evolution of the pressure coefficient $C_p = (P_e - P_{amb})/(0.5\rho U_0^2)$ along the channel is shown in Figure 4 for three transverse positions, in the APG configuration with $U_0 = 50$ m.s$^{-1}$. The mean flow appears to be homogeneous in the middle part of the channel, and the longitudinal profile of $C_p$ can be fitted with $C_p(x) = 1 \pm [L_0/(L_0 - x)]^2 + \text{cst}$.

Velocity measurements inside the channel have been performed using hot-wire anemometry for increasing speed $U_0$ from 25 to 100 m.s$^{-1}$. Only the case $U_0 = 50$ m.s$^{-1}$ is discussed hereafter. The local free-stream velocity $U_\infty$ at $x_{ref}$ is 38, 45 and 63 m.s$^{-1}$

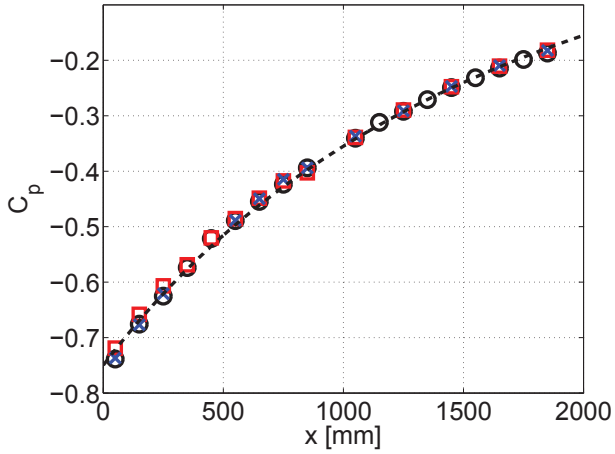


FIGURE 4 – Evolution of the pressure coefficient $C_p$ along the channel for three transverse positions : ∘ $y = 0$, × $y = -150$ mm and □ $y = 150$ mm, with $U_0 = 50$ m.s$^{-1}$, APG configuration. The dashed line corresponds to the longitudinal evolution of $C_p$ for an inviscid flow.

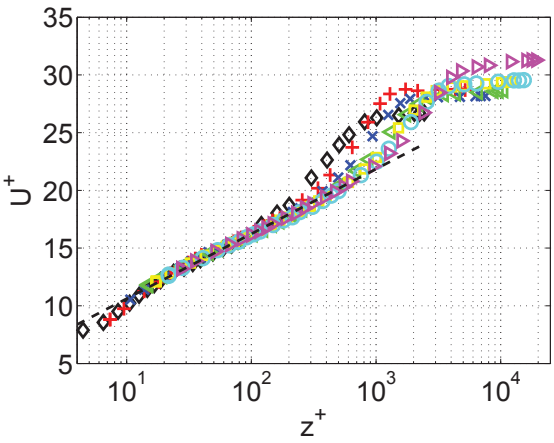


FIGURE 5 – Mean velocity profiles, expressed in wall units : ◇ $U_0 = 10$ m.s$^{-1}$, + $U_0 = 25$ m.s$^{-1}$, × $U_0 = 35$ m.s$^{-1}$, ◁ $U_0 = 50$ m.s$^{-1}$, □ : $U_0 = 60$ m.s$^{-1}$, ∘ $U_0 = 75$ m.s$^{-1}$, ▷ $U_0 = 100$ m.s$^{-1}$, - - - - logarithmic-law.

for the APG, ZPG and FPG case, respectively. The boundary-layer thickness $\delta$ is respectively 48, 26 and 18 mm, and values of the displacement thickness $\delta_1$ are respectively 5.5, 3.7 and 1.8 mm. The Reynolds number $R_{e\delta_1}$ based on the displacement thickness is respectively $13.7\times10^3$, $10.9\times10^3$ and $7.4\times10^3$ for the three mentioned configurations APG, ZPG and FPG. The friction velocity has been deduced from the logarithmic-law velocity profile, shown for the APG case in Fig. 5 for increasing speed $U_0 = 10$ m.s$^{-1}$ to 100 m.s$^{-1}$, where $U^+ = U/u_\tau$ and $z^+ = zu_\tau/\nu$. A logarithmic-law is observed in the range $10 < z^+ < 300$ approximately, depending on the free-stream velocity. With $U_0 = 50$ m.s$^{-1}$, values of the friction velocity are 1.34, 1.65 and 2.35 m.s$^{-1}$, for the APG, ZPG and FPG case respectively. Values of the gradient parameter $\beta = (\delta_1/\rho u_\tau^2)\, dP_e/dx$ are 0.94, 0 and -0.37 for the three mentioned configurations.

# 3 Data processing

A brief overview of the signal processing is given in what follows. The Fourier transform $\hat{p}(\boldsymbol{k},\omega)$ of the pressure field $p(\boldsymbol{x},t)$ in space and in time is defined by

$$p(\boldsymbol{x},t) = \iint \hat{p}(\boldsymbol{k},\omega) e^{i(\boldsymbol{k}\cdot\boldsymbol{x}-\omega t)} d\boldsymbol{k} d\omega = \mathcal{F}^{-1}\left\{\hat{p}(\boldsymbol{k},\omega)\right\}$$

Assuming stationary random signals and ergodicity, the cross spectral density is defined as,

$$R(\boldsymbol{x}_0,\boldsymbol{r},\omega) = \lim_{T\to\infty} \frac{2\pi}{T} E\left[\hat{p}(\boldsymbol{x}_0,\omega)\hat{p}^{\star}(\boldsymbol{x}_0+\boldsymbol{r},\omega)\right]$$

where $\boldsymbol{r}$ is the separation vector between two probes at $\boldsymbol{x}_0$ and $\boldsymbol{x}_0+\boldsymbol{r}$. In practice, the wall pressure field is assumed to be homogeneous over the microphone array, that is $R(\boldsymbol{x}_0,\boldsymbol{r},\omega) = R(\boldsymbol{r},\omega)$. Time signals are splitted into $m_t$ blocks $p_m$ of time length $T$. Using a rectangular windows, one has

$$R(\boldsymbol{r},\omega) = \frac{2\pi}{T}\frac{1}{m_t}\sum_{m=1}^{m_t} \hat{p}_m(\boldsymbol{r}_0,\omega)\hat{p}_m^{\star}(\boldsymbol{x}_0+\boldsymbol{r},\omega)$$

The wavevector - frequency spectrum is then directly computed by discretizing the following Fourier integral,

$$\Phi(\boldsymbol{k},\omega) = \frac{1}{(2\pi)^2}\iint R(\boldsymbol{r},\omega) e^{-i\boldsymbol{k}\cdot\boldsymbol{r}} d\boldsymbol{r}$$

The transducer locations are defined from the rotation of a linear antenna, as explained in the next section, and can thus be denoted $\boldsymbol{x}_{nm} = (d_n, m\Delta\theta)$ in polar coordinates. Hence,

$$\Phi(\boldsymbol{k},\omega) = \frac{1}{(2\pi)^2}\sum_{m=1}^{m_\theta}\sum_{n=0}^{n_r} R(\boldsymbol{r}_{nm},\omega) e^{-i\boldsymbol{k}\cdot\boldsymbol{r}} ds_{nm} \qquad (3)$$

with $\boldsymbol{k} = (k_x, k_y)$, and $\boldsymbol{k}\cdot\boldsymbol{r} = k_x d_n \cos\theta_m + k_y d_n \sin\theta_m$. The elementary area is given by

$$ds_{nm} = \pi(l_{n+1}^2 - l_n^2) \times \frac{\Delta\theta}{2\pi} \qquad l_n = \frac{d_n + d_{n+1}}{2}$$

# 4 Preliminary results

The power spectra obtained with the pinhole microphone have been scaled using mixed variables : the wall shear stress$\tau_w = \rho u_\tau^2$ as pressure scale and $\delta_1/U_\infty$ as timescale (see Fig. 6). An $\omega^{-1}$ decay of the spectrum amplitude is observed in the range $0.6 < \omega\delta_1/U_\infty < 6$ for the APG case ($\beta$=0.94). For the ZPG case ($\beta$=0), as mentioned by Goody [10], an $\omega^{-0.7}$ decay can be identified in the range $0.5 < \omega\delta_1/U_\infty < 3$. In the last case, FPG ($\beta$=-0.37), in the range $0.4 < \omega\delta_1/U_\infty < 1.5$ an amplitude decay as $\omega^{-0.2}$ is observed.

As an illustration, the wavevector - frequency spectrum measured for the case of a zero-pressure-gradient boundary layer at $U_0 = 50$ m.s$^{-1}$ is displayed in fig. 7 for two frequencies $f = 500$ Hz and $f = 1000$ Hz. As expected, the convective ridge is centered around the convective wavenumber $k_c = 2\pi f/U_c$ and is thus shifted to the right as the frequency is increased. An acoustic component can also be distinguished if $|\boldsymbol{k}| < \omega/c_0$.

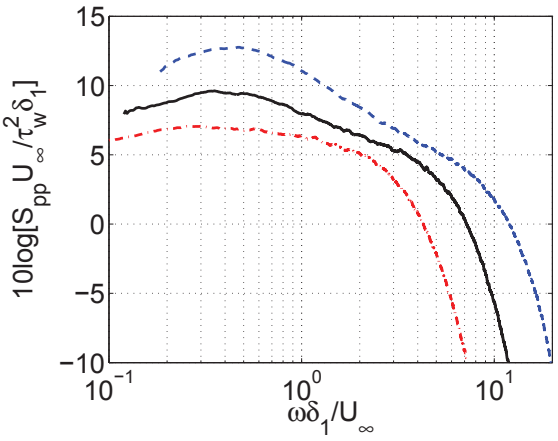


FIGURE 6 – Measured pressure spectra, for $U_0 = 50$ m.s$^{-1}$, scaled by $\tau_w$ as pressure scale and $\delta_1/U_\infty$ as timescale : - - - APG case $\beta$=0.94, ——— ZPG case $\beta$=0 and -.-. FPG case $\beta$=-0.37.

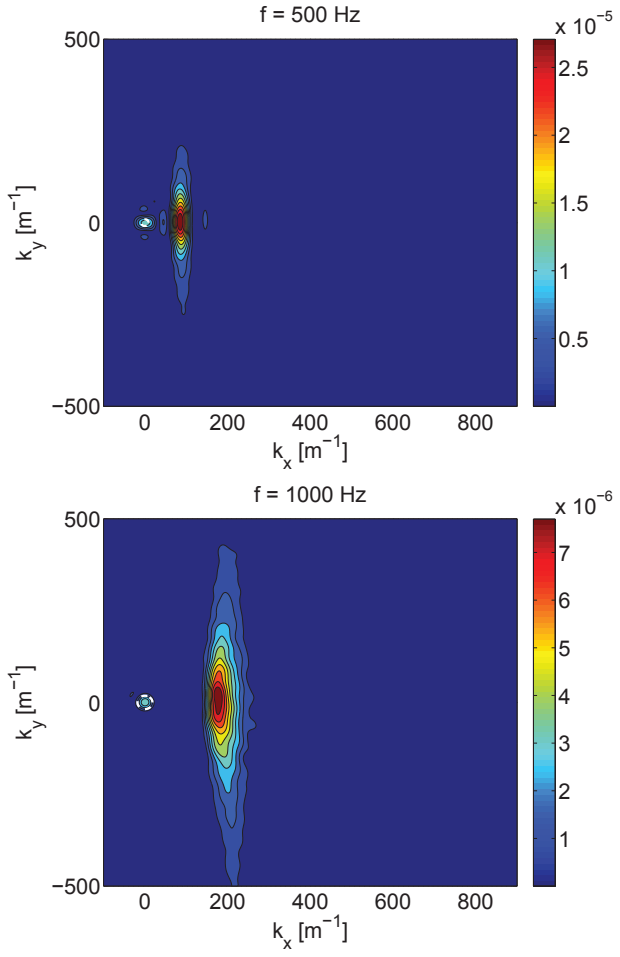


FIGURE 7 – Measured wavevector-frequency spectrum $\Phi(\boldsymbol{k},\omega)$ for the ZPG case, at $U_0 = 50$ m.s$^{-1}$, for two frequencies $f = 500$ Hz and $f = 1000$ Hz.

# 5 Concluding remarks

A new experimental facility has been designed to investigate turbulent boundary layers with a pressure gradient. Improvements of the wall-pressure instrumentation used in a previous study [1] have been implemented. Measurements for all the mentioned

configurations have been performed and briefly reported in the present paper. The shape of the wall-pressure spectrum has been discussed, regarding the value of the gradient parameter. An acoustic component in the wavenumber-frequency spectra is observed.

A more complete study will be presented [22], including detailed validations regarding turbulent boundary layers and pressure spectra. An estimation of the acoustic contribution to the wall-pressure fluctuations will also be proposed.

## Acknowledgments

The authors wish to express their most sincere thanks to Pascal Souchotte, Jean-Michel Perrin and Pierre Roland for their help in setting up the experiment. This research has been funded by the Agence Nationale de la Recherche through the ANR-2011-BS09-035-02 project SONOBL, and performed within the framework of the Labex CeLyA of Université de Lyon, operated by the French National Research Agency (ANR-10-LABX-0060/ ANR-11-IDEX-0007).

## Références

[1] Arguillat, B., Ricot, D., Bailly, C. & Robert, G., 2010, Measured wavenumber - frequency spectrum associated with acoustic and aerodynamic wall pressure fluctuations, *J. Acoust. Soc. Am.*, **128**(4), 1647-1655.

[2] Bremner, P. G. & Wilby, J. F., 2002, Aero-vibro-acoustics : problem statement and methods for simulation-based design solution, *8th AIAA/CEAS Aeroacoustics Conference*, AIAA Paper 2002-2551.

[3] Bull, M. K., 1996, Wall-pressure fluctuations beneath turbulent boundary layers : some reflections on forty years of research, *J. Sound Vib.*, **190**(3), 299-315.

[4] Cipolla, K. & Keith, W., 2000, Effects of pressure gradients on turbulent boundary layer wave number frequency spectra, *AIAA Journal*, **38**(10), 1832-1836.

[5] Corcos, G. M., 1963, Resolution of pressure in turbulence, *J. Acous. Soc. Am.*, **35**(2), 192-199.

[6] Corcos, G. M., 1964, The structure of the turbulent pressure field in boundary-layer flows, *J. Fluid Mech.*, **18**(3), 353-378.

[7] Ehrenfried, K. & Koop, L., 2008, Experimental study of pressure fluctuations beneath a compressible turbulent boundary layer, *14th AIAA/CEAS Aeroacoustics Conference*, AIAA Paper 2008-2800.

[8] Gabriel, C., Müller, S., Ullrich, F. & Lerch, R., 2013, Measurement of the spatial coherence of surface pressure in the wake of a car's side mirror, 19th AIAA/CEAS Aeroacoustics Conference, AIAA Paper 2013-2059.

[9] Gloerfelt, X. & Berland, J., 2013, Turbulent boundary-layer noise : direct radiation at Mach number 0.5, *J. Fluid Mech.*, **723**, 318-351.

[10] Goody, M., 2004, Empirical spectral model of surface pressure fluctuations, *AIAA Journal*, **42**(9), 1788-1794.

[11] Graham, W. R., 1997, A comparison of models for the wavenumber-frequency spectrum of turbulent boundary layer pressures, *J. Sound Vib.*, **206**(4), 430-454.

[12] Hu, Z., Morfey, C. L. & Sandham, N. D., 2006, Sound radiation from a turbulent boundary layer, *Phys. Fluids*, **18, 098101**, 1-4.

[13] Keith, W. L., Hurdis, D. A. & Abraham, B. M., 1992, A comparison of turbulent boundary layer wall-pressure spectra, *Journal of Fluids Engineering*, **114**, 338-347.

[14] Leclercq, D. J. J. & Bohineust, X., 2002, Investigation and modelling of the wall pressure field beneath a turbulent boundary layer at low and medium frequencies, *J. Sound Vib.*, **257**(3), 477-501.

[15] Maidanick, G., 1967, Flush-Mounted pressure transducer systems as spatial and spectral filters, *J. Acoust. Soc. Am.*, **42**(5), 1017-1024.

[16] Nélisse, H. & Nicolas, J., 1997, Characterization of a diffuse field in a reverberant room, *J. Acoust. Soc. Am.*, **101**(6), 3517-3524.

[17] Ollivier, S., Salze, E., Averiyanov, M., Yuldashev, P., Khokhlova, V., & Blanc-Benon, P., 2012, Calibration method for high frequency microphones, *Acoustics 2012, 11ème Congrès Français d'Acoustique & 2012 Annual IOA (Institute of Acoustics, UK)*, 13-17 April, Nantes, 3503-3507.

[18] Panton, R. L. & Robert, G., 1994, The wavenumber-phase velocity representation for the turbulent wall-pressure spectrum, *Journal of Fluid Engineering*, **480**(116), 477-483.

[19] Rozenberg, Y., Robert, G. & Roger, M., 2012, Wall-pressure spectral model including the adverse pressure gradient effects, *AIAA Journal*, **50**(10), 2168-2179.

[20] Schloemer, H. H., 1967, Effects of pressure gradient on turbulent-boundary-layer wall-pressure fluctuations, *J. Acoust. Soc. Am.*, **42**(1), 93-113.

[21] Salze, E., Ollivier, S., Blanc-Benon, P., Yuldashev, P., Averiyanov, M., & Khokhlova, V., 2011, Characterisation of the sound field emitted by an electric spark source in air, *6th Forum Acusticum*, ACUSTICUM2011/285 Aalborg, Denmark, June 27-July 1st.

[22] Salze, E., Bailly, C. Marsden, O., Jondeau, E. & Juvé, D., 2014, An experimental characterisation of wall pressure wavevector-frequency spectra in the presence of pressure gradients, *20th AIAA/CEAS Aeroacoustics Conference*, June 16-20th 2014, Atlanta (accepted).

[23] Wilby, J. F., 1996, Aircraft interior noise, *J. Sound Vib.*, **190**(3), 545-564.